frontiers | Frontiers in Earth Science

TYPE Original Research
PUBLISHED 25 July 2024
DOI 10.3389/feart.2024.1403575

OPEN ACCESS

EDITED BY
Hu Li,
Sichuan University of Science and Engineering, China

REVIEWED BY
Yifan Gu,
Southwest Petroleum University, China
Qingguang Li,
Guizhou University, China

*CORRESPONDENCE
Junfeng Cao,
cjinyan006@126.com

RECEIVED 19 March 2024
ACCEPTED 28 June 2024
PUBLISHED 25 July 2024

CITATION
Zhang H, Cao J, Lan B, Chen Y, Zhang Q, Men Y, Feng X and Yu Q (2024), Organic matter enrichment model of Permian Capitanian-Changhsingian black shale in the intra-platform basin of Nanpanjiang basin. *Front. Earth Sci.* 12:1403575. doi: 10.3389/feart.2024.1403575

Organic matter enrichment model of Permian Capitanian-Changhsingian black shale in the intra-platform basin of Nanpanjiang basin

Haiquan Zhang[1,2], Junfeng Cao[1,2]*, Baofeng Lan[3], Yi Chen[4], Qian Zhang[1,2], Yupeng Men[1,2], Xintao Feng[1,2] and Qian Yu[1,2]

[1]Chengdu Center of China Geological Survey, Geosciences Innovation Center of Southwest China, Chengdu, China, [2]Key Laboratory of Sedimentary Basin and Oil and Gas Resources, Ministry of Natural Resources, Chengdu, China, [3]Guizhou Energy Industry Research Institute Co., Ltd., Guiyang, China, [4]Guizhou Research Institute of Petroleum Exploration and Development, Guiyang, China

The Permian Capitanian-Changhsingian black shale formed in intra-platform basins are the major source rocks in Southwest China. However, the depositional conditions and organic matter accumulation of these black shales are not well understood. In this study, geochemical characteristics comprise TOC, major, trace and REEs from sixty-two samples from the studied outcrop in Northern Nanpanjiang Basin, Southwest China are systematically investigated to determine silicon source, paleo-ocean productivity, and paleo-redox conditions to reveal their influence on organic matter enrichment under 3rd-order sequence. The Capitanian-Changhsingian black shale in the study area is the result of the combined effects of active extensional activity, high paleo-productivity maintained by volcanic activity, and dysoxic and anoxic conditions represented by biological extinction events. There are differences in the factors controlling organic matter accumulation in black shale at different stages. The controlling factors for the organic enrichment during Capitanian (SQ2) are the rapidly deepening water mass of extensional rifts and the high productivity induced by volcanic ash in the igneous provinces, as well as the global anoxic event represented by "negative carbon isotope shift." The controlling factors during Changhsingian are the deepening of water mass under the reactivation of extensional rifts, resulting in a dysoxic environment, and the high productivity maintained by volcanic activity in South China. The Wuchiapingian black shale was formed under dysoxic conditions under the stagnation of extensional activity, and intermittent volcanic activity in South China maintained the high paleo-productivity level of the Wuchiapingian stage.

KEYWORDS

Permian Capitanian, organic matter, enrichment model, black shale, intra-platform basin, Nanpanjiang basin

Introduction

With the development of advanced geochemical indices of elements (Algeo and Maynard, 2004; Zhao et al., 2016; Wei et al., 2022), the paleoenvironmental conditions

and organic matter enrichment mechanism of black organic-rich shale have become a research hotspot in recent years (Qiu and Zou, 2020; Gu et al., 2022; Liu et al., 2022). Shale deposited under different formation environments show significant differences in mineral composition, organic matter types, and sweet spot distribution (Li, 2023; Fan et al., 2024; Liu et al., 2024), which in turn affect the various performance characteristics of shale reservoirs (Loucks et al., 2009; Ross and Marc Bustin, 2009; Labani et al., 2013). Affected by the successful exploration of shale oil and gas in North America (Jiang et al., 2016; Jiang et al., 2018; Zou et al., 2019; Cai et al., 2023a), the Chinese Ministry of Land and Resources has conducted a survey and evaluation of the potential shale gas resources throughout China (Bai et al., 2023; Cai et al., 2023b; Fang et al., 2023; Wang et al., 2023). In recent years, the Permian black shale of transitional, and lacustrine in China have achieved industrial production capacity and are expected to form large-scale production capacity, becoming a new field for shale gas production on a large scale (Dong et al., 2021; Lin et al., 2021; Jiao et al., 2023). However, influenced by the complexity of the geological background (Mei et al., 2007; Shen et al., 2019), research on the Permian marine shale is rare.

Organic matter accumulation is a complex physical-chemical process that involves many factors, such as redox condition of bottom seawater, sedimentation rate, productivity of surface water, and geological event (Hu et al., 2018; Gu et al., 2022; Tan et al., 2024). The main controlling factors for organic matter enrichment in modern and paleo marine sediments have been extensively discussed over the past 30 years (Pedersen et al., 1990; Arthur and Sageman, 1994; Wei et al., 2012; Ding et al., 2018). Currently, the controlling factors for organic matter enrichment can be summarized as primary productivity and favorable preservation conditions. The productivity school believes that organic matter accumulation is mainly controlled by the biological productivity of the ocean surface, and the impact of water redox properties is limited. The typical representative is the rising ocean currents on the continental margin. The oxidation-reduction school believes that low marine surface productivity can also form organic rich sediments in hypoxic environments, especially in sulfide environments, with modern anoxic basins such as the Black Sea and Cretaceous marine anoxic events as typical representatives. Moreover, few scholars believe that an appropriate sedimentation rate is the key factor causing organic matter enrichment, and either too high or too low sedimentation rates are not conducive to organic matter enrichment.

At present, organic matter content plays a crucial role in shale hydrocarbon enrichment (Han et al., 2021; Zhang et al., 2022). Therefore, in the early stage of shale resource exploration, it is necessary to identify the mechanism of organic matter enrichment. The type and abundance of organic matter are the results of sedimentary processes, which are controlled by environmental conditions (Tribovillard et al., 2012; Zhang et al., 2018). Based on the geochemical analysis of the Permian marine shale in the Nanpanjiang Basin, this study elaborates on the environmental sensitivity indicators of black shale formed in the intra-platform basin, analyzes the impact of geological events on the shale sedimentary environment, and establishes an organic matter enrichment model for black shale in the intra-platform basin.

Geological setting

The studied outcrop is located in the southern Ziyun area (Figure 1A), Nanpanjiang Basin. During the Permian period, the outcrop belonged to the Nanpanjiang sedimentary division of the South China platform basin sedimentary system (Peng et al., 2006). Under the background of late Paleozoic extensional subsidence, the Nanpanjiang Basin formed a passive continental margin rift type basin, forming a special sedimentary pattern of connected continental platforms, shallow water isolated platforms, and intra platform basins within the basin (Peng et al., 2006; Yin et al., 2014). The studied outcrop is located in a basin within the carbonate platform, representing a deep-water sedimentary sequence (Wang et al., 2022). In the late Middle Permian to early Late Permian, the area where this outcrop was located was strongly affected by the rapid uplift of the crust dome caused by the impact of the Emeishan mantle plume on the bottom of the lithosphere. In the transitional zone between the relatively uplifted and relatively subsidence areas (Zhai et al., 2020), crustal activity was outcrop, and a large amount of volcanic material was deposited in the deep-water sediments of this section, manifested as frequent interbeddings of bentonite in black marine shale (Lai et al., 2008; Gu et al., 2022). Based on lithological combinations and biological zoning, the Guadalupian-Lopingian of the studied outcrop can be divided into four stages (Figure 1B), corresponding to four third-order sequences (Mei et al., 2007). The Wordian stage comprises medium-bedded bioclastic limestone. The Capitanian stage comprises siliceous and clayey black shale abundant with fossils of radiolarians and foraminifera (Figure 2). The Wuchiapingian strata is composed of silty mudstone, siltstone and shale intercalated with thin-bedded limestone. The lower strata of Changhsingian stage comprises limestone, bioclastic limestone and organic-poor mudstone. The upper Changhsingian stage comprise black shale intercalated with thin-bedded limestone.

Samples and methods

Sample collection

This study conducted a careful field investigation on the studied profiles and sampled them layer by layer, totaling 62 shale samples. During the collection process, avoid areas with severe weathering effects to ensure that all samples come from fresh surfaces. Make all samples into thin sections to observe microscopic characteristics. Using an agate mortar, the remaining portion of the shale sample was ground into a 200 mesh powder for elemental geochemical testing and total organic carbon (TOC) testing.

TOC measurement

The total organic carbon content is not only an important part of improving organic carbon isotope stratigraphy, but also plays an important role in evaluating source rock quality. The samples pre-treated with the aforementioned organic carbon isotopes were subjected to sufficient combustion in an environment of high temperature and pure oxygen flow. Subsequently, strong oxidants were used to react in acidic solutions, and the collected CO_2 gas

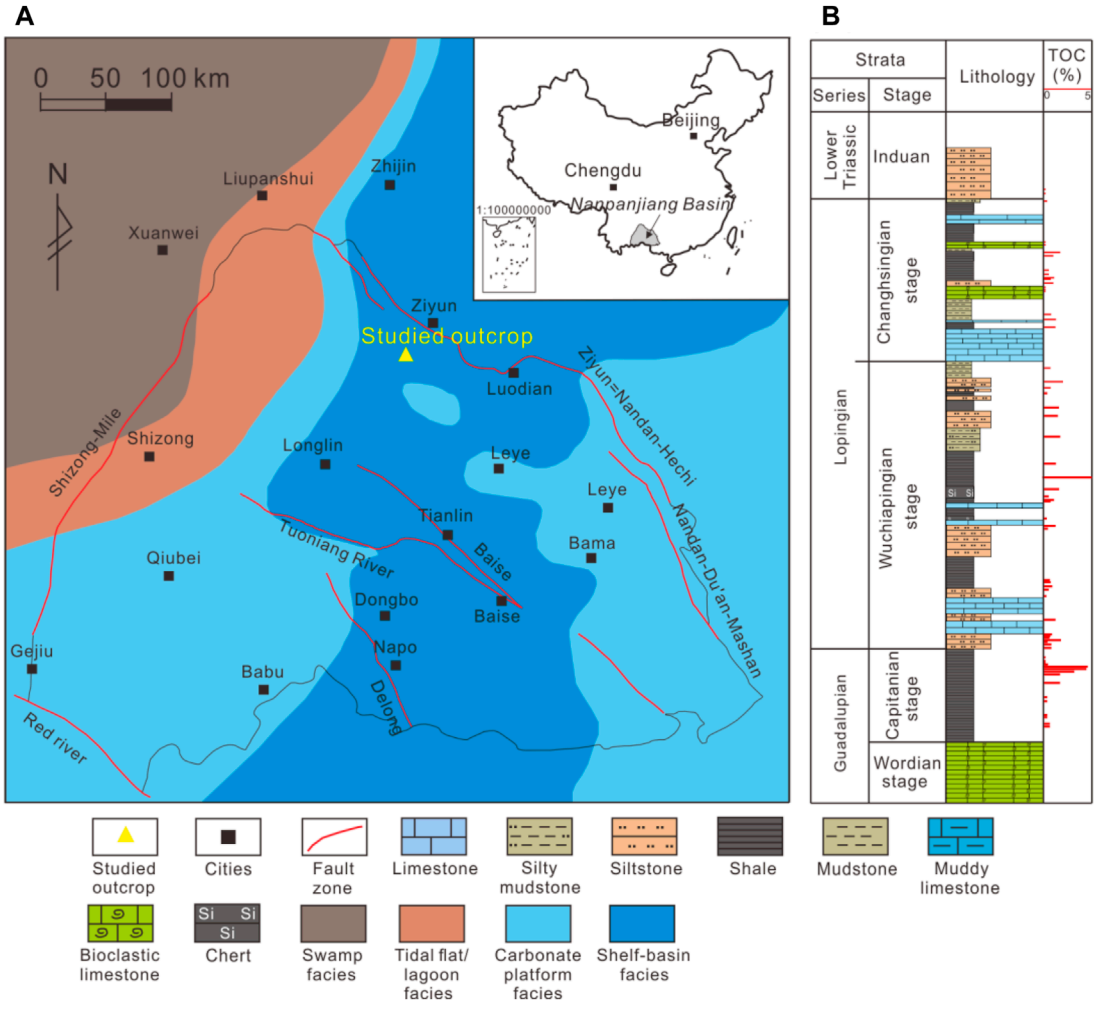

FIGURE 1
(A) Sedimentary environment of Nanpanjiang Basin during Permian Capitanian-Changhsingian (modified from Gu et al., 2022). **(B)** Generalized stratigraphy of Guadalupian-Lower Triassic strata of the studied outcrop.

was purified in a vacuum system to remove interfering substances. Although the instrument calculated the content of organic carbon by measuring the content of CO_2. The TOC measurement was carried out using the Elemental VarioMACRO CHNS elemental analyzer in the Key Laboratory of Unconventional Oil and Gas of PetroChina at Southwest Petroleum University.

Bulk element concentration

The major elements were measured by using the PE ELAN DRC-E type ICP-MS (Inductively Coupled Plasma Mass Spectrometry) made in the United States, and the $Li_2B_4O_7$ and $LiBO_2$ (67:33) mixed flux was used to melt samples with the high-temperature automatic gas sample machine of Glaisse in Canada. The test conditions are: X-ray working voltage 40 kV current 60 rnA, analysis accuracy better than 5%.

Trace Elements and Rare Earth Elements (REE): Dry a 200 mesh sample in an oven at 105°C. After drying, weigh 25 mg of the sample and place it in a high-pressure dissolution tank called Teflon. Add 0.5 mL of concentrated HF, heat and evaporate to dryness at 120°C. After removing some of the sample for 1 day, add 1 mL of concentrated HF and 0.5 mL of concentrated HNO_3. Place the PTFE inner tank in a steel sleeve, tighten it, and heat it in a 190°C oven for 2,448 h. Dissolve the sample and evaporate it to dryness at 120°C until it becomes a wet salt, Add 1 mL of HNO_3 and evaporate to a wet salt state at 140°C to remove excess HF from the sample. Finally, add 5 mL of 30% (v/v) HNO_3, seal and heat at 140°C for 4 h. After cooling, add 1 mL of 500 ng/mL Rh internal standard solution and dilute to 50 mL. The instrument used in the experiment is the Finnigan Element 2 mass spectrometer, and the Millipore water purification system Milli-Q is used to prepare 18 M Ω. Ultra pure water, sample treatment is carried out in a Class 100 ultra clean laboratory. The error is less than 10%. The determination of trace elements and rare earth elements was carried out using ICP-MS with an error of less than 5%.

X-ray diffraction

Extract <2 from each shale sample using sedimentation method μ M clay particles are made into directional sheets. First, rinse

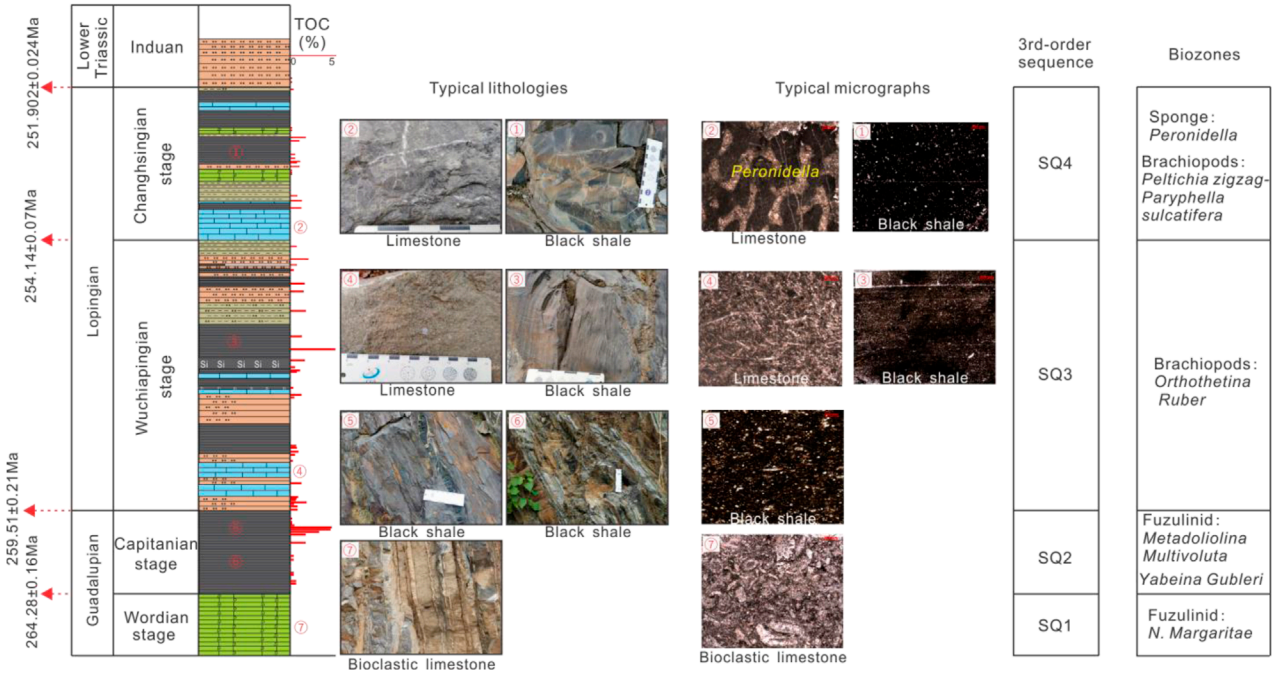

FIGURE 2
Comprehensive stratigraphic column for the Guadalupian-Lower Triassic in the studied outcrop. Sequence column is from Mei et al. (2007). Biozones are from National Commission on Stratigraphy of China (Wang et al., 2014).

repeatedly with distilled water, then place it in a 2000 mL quartz beaker, add 1,500 mL of distilled water and mix thoroughly. After 20 h at 25°C, the upper part of the solution should be <2 μ The suspension is sucked into a centrifuge tube and centrifuged at 2,500 rpm for 10 minutes. The sediment at the bottom of the centrifuge tube is <2 μ Sample of m particles. Add 2 mL of distilled water and apply the emulsified mud like sample onto two 20 –30 cm flat glass plates to make directional plates, which are then dried naturally and treated with ethylene glycol. When treating the sample with ethylene glycol, steam method is used at a temperature of 600 and heated for about 12 h. The instrument used is the Broker D8 Advance X-ray powder diffractometer, Cu target, instrument voltage 4.0 kV, tube current 40 mA, scanning speed 250/min, scanning step width 0.0167°, scanning range 3°–25° (2 θ).

Results

Major elements

The chemical composition of the Capitanian black shale in the studied outcrop is mainly SiO_2, with a content of 37.0%–65.0%, an average of 52.9%, followed by Al_2O_3 and TFe_2O_3, with an average content of 15.2% and 9.6%, respectively. The remaining oxides include MgO, CaO, Na_2O, K_2O, TiO_2, and MnO, with average contents of 2.5%, 3.5%, 1.1%, 2.3%, 2.6%, and 0.2%, respectively. The SiO_2 content of black shale in the Wuchiapingian-Changhsingian stage ranges from 37.9% to 55.3%, with an average value of 45.2%, which is significantly lower than that of the Capitanian shale. The average content of Al_2O_3 and TFe_2O_3 is 13.4% and 11.6%, respectively. The other oxides include MgO, CaO, Na_2O, K_2O, TiO_2, and MnO, with an average content of 3.1%, 7.8%, 2.1%, 1.9%, 2.6%, and 0.2%, respectively. The SiO_2 content of the Ordovician-Silurian black shale in South China ranges from 28.3% to 81.7%, with an average value of 60.0%. The average contents of Al_2O_3 and TFe_2O_3 are 12.7% and 4.9%, respectively. The other oxides include MgO, CaO, Na_2O, K_2O, TiO_2, and MnO, with average contents of 2.4%, 3.7%, 1.1%, 3.5%, 0.6%, and 0.03%, respectively. In contrast, in terms of SiO_2 content, the Ordovician-Silurian black shale is higher than the Capitanian shale, and the Wuchiapingian-Changhsingian shale are the lowest. In terms of TiO_2 and MnO content in shale, the Capitanian, Wuchiapingian-Changhsingian shale are significantly higher than the Ordovician-Silurian shale (Table 1).

The Capitanian black shale sample has a high loss on ignition (average 12.8%), and the Wuchiapingian-Changhsingian black shale also has a high loss on ignition (average 12.1%). The $SiO_2/(K_2O + Na_2O)$ values of Capitanian black shale range from 10.6 to 55.2, with an average of 19.7. The value distribution of SiO_2/Al_2O_3 ranges from 2.2 to 5.3, with an average value of 3.7. The value of $(K_2O + Na_2O)/Al_2O_3$ ranges from 0.1 to 0.3, with an average value of 0.2. The value distribution of MnO/TiO_2 ranges from 0.02 to 0.2, with an average value of 0.1. The $SiO_2/(K_2O + Na_2O)$ values of the Wuchiapingian-Changhsingian black shale range from 9.4 to 18.3, with an average of 12.4. The value distribution of SiO_2/Al_2O_3 ranges from 2.8 to 6.1, with an average value of 4.0. The value of $(K_2O + Na_2O)/Al_2O_3$ ranges from 0.3 to 0.4, with an average value of 0.3. The value distribution of MnO/TiO_2 ranges from below 0.1 to 0.2, with an average value of 0.1.

TABLE 1 Comparison of major elements average (%) in black shales among different Formation.

Strata/Stage	SiO_2	Al_2O_3	TFe_2O_3	MgO	CaO	Na_2O	K_2O	TiO_2	MnO
Wuchiapingian-Changhsingian	52.91	15.22	9.56	2.47	3.49	1.07	2.26	2.55	0.15
Capitanian	45.24	13.39	11.58	3.05	7.83	2.12	1.88	2.55	0.19
Ordovician-Silurian	59.98	12.71	4.91	2.35	3.69	1.09	3.51	0.63	0.03

Trace and rare earth elements

The Capitanian black shale sample has a V content between 77.8×10^{-6}–344.0×10^{-6}, with an average of 188.27×10^{-6}. In the black shale of Changhsingian, the average V content increases to 229.0×10^{-6}. The Mo content in the black shale of Capitanian is between 0.6×10^{-6}–5.0×10^{-6}, with an average of 2.02×10^{-6}. The Mo value of black shale in the Changhsingian stage increased to 9.71×10^{-6}. The Cr distribution of Capitanian black shale ranges from 14.9×10^{-6} to 136.6×10^{-6}, with an average of 76.1×10^{-6}. The Cr value of Changhsingian black shale is significantly higher, distributed between 76.0×10^{-6} and 287.0×10^{-6}, with an average of 160.8×10^{-6}. The Ba content of the Capitanian black shale is distributed between 88.85×10^{-6}–623.96×10^{-6}, with an average of 354.31×10^{-6}. The Ba content of the black shale belonging to Changhsingian stage is distributed between 239.0×10^{-6}–$2{,}289.0 \times 10^{-6}$, with an average of 723.4×10^{-6}.

The distribution range of ∑REE in the black shale sample of Capitanian is 46.32×10^{-6}–941.85×10^{-6}, with an average value of 357.27×10^{-6}. The ∑REE distribution range of the Changhsingian black shale sample is 143.94×10^{-6}–416.86×10^{-6}, with an average value of 284.53×10^{-6}.

Discussions

The distribution characteristics of organic matter and silicon components can intuitively reflect the close relationship between the lithological changes and organic matter content of organic-rich shale. In addition, it also indicates that in order to reveal the synchronous coupling mechanism between organic matter enrichment and silicon enrichment in the formation, it is necessary to first clarify the source and origin of silicon components in shale, and then identify the symbiotic coupling mechanism that determines the synchronous enrichment of organic matter and silicon. The measurement results suggest that the major elemental composition of Capitanian shale, Wuchiapingian shale, and Changhsingian shale is similar to the characteristics of siliceous rocks formed by volcanic biochemical processes (Table 2). High values of loss on ignition are related to the rich organic matter in the shale samples. There is a significant difference in the background values of the parameters and hydrothermal genesis of the Capitanian, Wuchiapingian - Changhsingian black shale (Table 2).

Yamamoto (1987) proposed that hot water activity can lead to the enrichment of Fe and Mn elements. After analyzing 42 Cretaceous rock samples from the North Pacific, Adachi et al. (1986) proposed that the enrichment of TFe_2O_3 is an important feature of hydrothermal silica. The TFe_2O_3 content in the black shale is not high, and the Capitanian black shale is distributed between 1.3% and 12.8%, with an average of only 9.8%. The MnO content is extremely low, with an average of only 0.2%. The TFe_2O_3 content in the Wuchiapingian-Changhsingian black shale is also not high, ranging from 4.9% to 14.8%, with an average value of only 11.3% and an average MnO content of only 0.2%, both of which do not have typical hydrothermal genesis characteristics.

The Al/(Al+Fe+Mn) value in marine sediments is a marker for measuring the content of hydrothermal components in sediments (Adachi et al., 1986). This ratio increases with the distance away from the expansion center, thereby distinguishing the contribution of hydrothermal components to sediments. The Al/(Al + Fe + Mn) values of hydrothermal sediments located in the eastern Pacific Ocean are mostly between 0.01 and 0.2, and their ratio is less than 0.35 due to the influence of hot water. The average ratio of hydrothermal silica collected from the North Pacific is 0.12, while the ratio of semi oceanic silica from the Kamiaso biogenic Triassic in central Japan is 0.60. The Al/(Al + Fe + Mn) values of black shale in the studied outcrop range from 0.43% to 0.59%, with an average of 0.52. The Al/(Al + Fe + Mn) value of Wuchiapingian-Changhsingian black shale ranges from 0.4% to 0.6%, with an average of 0.5, which is close to the value of pure biogenic silicon. On the Al Fe Mn triangulation, the majority of the samples from the Capitanian stage are located within the biogenic zone, with a few samples adjacent to the Wuchiapingian-Changhsingian stage (Figure 3). The silicon in the black shale of Capitanian, Wuchiapingian-Changhsingian in the studied outcrop is of non-hydrothermal origin, and the vast majority of Capitanian shale is biogenic silicon.

Mn in siliceous rocks is often considered as a marker element from the deep ocean (Sugisaki), and the MnO/TiO_2 ratio can be used as a marker to determine the distance of siliceous sediments from the ocean basin (Halamić et al., 2005). The ratio of siliceous rocks deposited on continental slopes and marginal seas closer to the continent should be less than 0.5, and siliceous sediments on open ocean bottoms can reach 0.5–3.5. The MnO/TiO_2 values in the Capitanian black shale in the studied outcrop are 0.02–0.2, with an average of 0.09. The MnO/TiO_2 values in the Wuchiapingian-Changhsingian black shale are 0.04–0.2, with an average of 0.09, suggesting that the siliceous rocks in the study area were formed in the sedimentary environment of the continental slope and marginal seas closer to the continent.

V and Mo are bioactive elements, and their high enrichment indicates that the formation of silicon in shale is related to biological activity. The Capitanian black shale sample shows a higher V content than the abundance of sedimentary rocks, which is 1.55 times higher. In the black shale of Changhsingian, the V value increases to 229 ×

10.3389/feart.2024.1403575

TABLE 2 Comparison of major elements in typical biogenic, hydrothermal, and volcanic mudstone/shale.

Major element proxy	Biogenic mudstone/shale		Hydrothermal mudstone/shale		Volcanic mudstone/shale	Volcanic-biogenic mudstone/shale
$Al/(Al + Fe + Mn)$	0.5	0.22	0.22	0.28	0.57	0.29
$SiO_2/(K_2O + Na_2O)$	872.36	258.94	159.7	111.8	35.75	82.44
SiO_2/Al_2O_3	135.15	104.81	65.7	45.63	13.66	23.05
$(K_2O + Na_2O)/Al_2O_3$	0.15	0.4	0.41	0.42	0.38	0.28
MnO/TiO_2	0.67	18.75	8.89	9.75	0.25	0.8

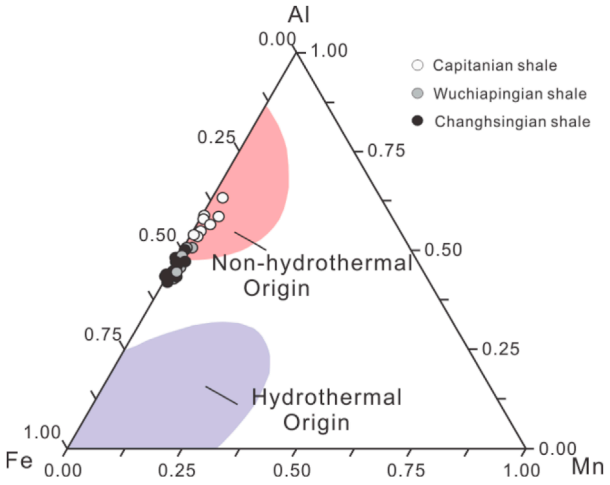

FIGURE 3
Al-Fe-Mn column Triangle diagram of black shale in the studied outcrop. Hydrothermal and non-hydrothermal fields are cited from Adachi et al. (1986).

10^{-6}. The Mo content in the black shale of Capitanian is slightly lower than that of sedimentary rocks. The Mo value of black shale in the Changhsingian stage increased to 9.71×10^{-6}. This could imply that the formation of black shale in this area exhibits strong biological effects, and the biological activity has significantly increased from the Capitanian stage to the Changhsingian stage.

Cr is a mantle friendly element with an average content of 76.3. The Cr distribution of Capitanian black shale is slightly higher than the abundance of sedimentary rocks at 63.0. And the Cr value of Changhsingian black shale is much higher than the abundance of sedimentary rocks of 63.0. This phenomenon can be attributed to the extensional movement of the Changhsingian stage, which led to the development of rising ocean currents near the fault zone, bringing in a large amount of Cr elements.

Siliceous sediments of hydrothermal origin are usually positively correlated with Ba and SiO_2. In generally, siliceous rocks of pure biogenic origin contain higher Ba content (Li et al., 2014). There is a weak negative correlation between Ba and SiO_2 in the black shale, with a correlation coefficient of −0.17 (Figure 4). The Ba content of the Capitanian black shale is slightly lower than the abundance of Ba in sedimentary rocks. The Ba content of the black shale belonging to Changhsingian stage is 1.57 times the abundance of Ba in sedimentary rocks. Therefore, it reflects a relatively strong biological activity, and the biological activity intensity of the Changhsingian black shale is significantly higher than that of the Capitanian black shale.

The overall ∑REE of siliceous sediments related to hydrothermal activity is relatively low, while siliceous rocks affected by terrestrial debris have relatively high ∑REE. The ∑REE distribution range of the Changhsingian black shale sample is generally higher than the standard shale (204.1×10^{-6}). REE is an important chemical tracer for restoring paleo-marine environments, distinguishing redox conditions, and distinguishing between hydrothermal or non-hydrothermal sediments. In general, hydrothermal sedimentary siliceous rocks have low ∑REE, significant loss of Ce, and

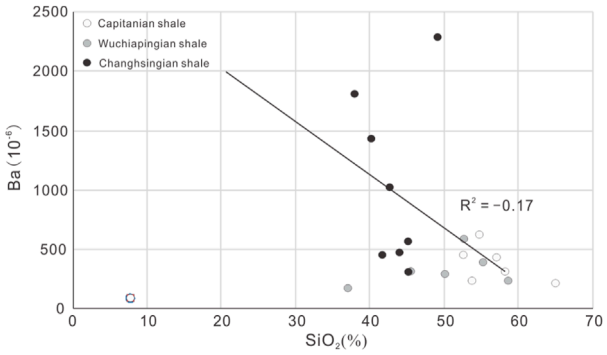

FIGURE 4
Correlation between Ba and SiO_2 of black shale in the studied outcrop.

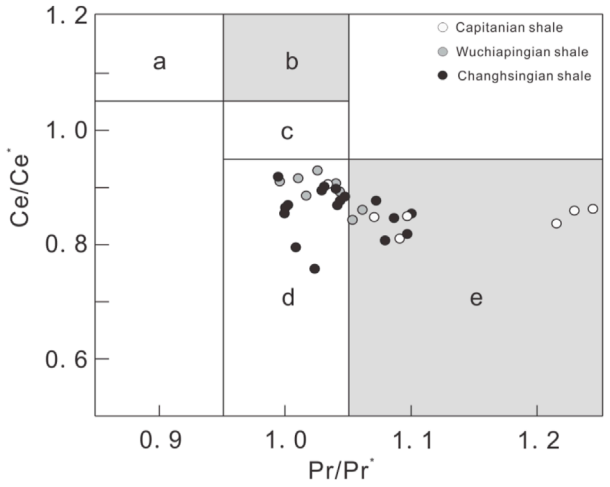

FIGURE 5
Cross-plot of Ce/Ce ∗ and Pr/Pr ∗ in the black shale. Zone a represents a positive anomaly in Ce. Zone b represents a negative La anomaly and no Ce anomaly. Zone c represents that both Ce and La are normal. Zone d represents a positive anomaly in La and no anomaly in Ce. Zone e represents negative Ce anomaly.

insignificant loss of Eu, even exhibiting Eu positive anomalies. However, the rare earth elements in non hydrothermal sedimentary siliceous rocks are similar to shale, relatively enriched in light rare earth elements The characteristics of LREE enrichment, ∑HREE non-enrichment, ∑LREE/∑HREE average value of 10.22, negative Ce anomaly, and weak positive Eu anomaly once again confirm that black shale does not belong to hydrothermal sedimentation.

Previous studies have shown that La enrichment exists in metal-rich sediments and high-temperature hydrothermal fluids, leading to the occurrence of negative Ce anomalies (Bao et al., 2008). Use Pr/Pr ∗ values to test for the occurrence of negative Ce anomalies caused by La enrichment. When Ce/Ce ∗ <1 and Pr/Pr ∗ ≈ 1, it indicates the occurrence of positive La anomalies (Figure 5, Zone d). According to the Ce/Ce ∗ - Pr/Pr ∗ plot of black shale, the data points are all located in the d and e zones, with Pr/Pr ∗ values greater than 1, indicating that the negative anomaly of Ce is not affected by the enrichment of La. Weak influence of high-temperature hydrothermal solution.

Therefore, the black shale in the studied outcrop is mainly biogenic, and the relative content of biogenic silicon and terrestrial detrital silicon can be quantitatively calculated and judged by the biogenic silicon content in various lithofacies. Previous studies suggested that the Post Archean Australia Shale (PAAS) represented the average chemical composition of the upper crust, and its source was typical terrestrial debris (Ma et al., 2017). Therefore, the value of $Al_2O_3 \times (SiO_2/Al_2O_3)_{PAAS}$ can be used to represent the silicon content of terrestrial debris in the study area, and the calculation formula is as follows:

$$\text{Bio}\,SiO_2(\%) = SiO_2 - Al_2O_3 \times (SiO_2/Al_2O_3)_{PAAS}$$

Bio SiO_2 represents the content of biogenic silicon, SiO_2 and Al_2O_3 represent the content of silica and alumina respectively, and $(SiO_2/Al_2O_3)_{PAAS}$ represents the ratio of silica and alumina in the Post Archean Australia Shale (PAAS). The results indicate that the content of biogenic silicon in black shale of study area accounts for 23.13%–80.90% of the total silicon. The average value of biogenic silicon is over 50% in terms of the total silicon.

Many researchers have conducted extensive research on the sources of silicon in shale and investigated the effects of terrestrial detrital silicon and biogenic silicon on TOC enrichment (Milliken et al., 2016; Milliken and Olson, 2017). As shown in Figure 6, there is a relationship between different types of silica and TOC: Devonian-Mississippian Muskwa and Besa River black shale, mainly composed of biogenic quartz (derived from siliceous radiolarians), have a sedimentary environment in the deep-water area outside the slope, and biogenic quartz has a high degree of correlation with TOC, indicating that biogenic silica has a significant contribution to the enrichment of TOC (Figure 6A).

The Ordovician-Silurian black shale is rich in biogenic silicon, characterized by synchronous changes in biogenic silicon and organic matter, with a correlation coefficient of up to 0.80 (Figure 6B), indicating that the sinking fluxes of organisms with siliceous skeletons have a significant enrichment effect on TOC (Ge et al., 2021; Xiong et al., 2021).

In order to more accurately reflect the relationship between silicon content and TOC, as well as the vertical evolution characteristics, this study conducted a correlation analysis between SiO_2 and TOC in black shale (Figure 7), indicating that there was no significant correlation between SiO_2 and TOC in the Permian black shale in the studied outcrop. Based on the observation of thin-sections, a large number of radiolarian individuals and fragments were observed in the Capitanian black shale. Silicon is mainly biogenic, and biogenic silicon mainly comes from radiolarians. The siliceous components of the black shale in Wuchiapingian and Changhsingian are mainly volcanic quartz silicon and terrestrial detrital silicon.

Previous studies have used the chemical composition ratios of siliceous rocks in known sedimentary environments to map and delineate the projection areas of siliceous rocks on continental margins, distant oceans, and mid ocean ridges (Wang et al., 2016). As shown in Figure 8, almost all samples fall into the continental margin area or are distributed adjacent to the continental margin. In summary, the consistent geochemical characteristics of black shale indicate that it was formed in an anoxic environment on the continental margin.

2021; Ge et al., 2021).

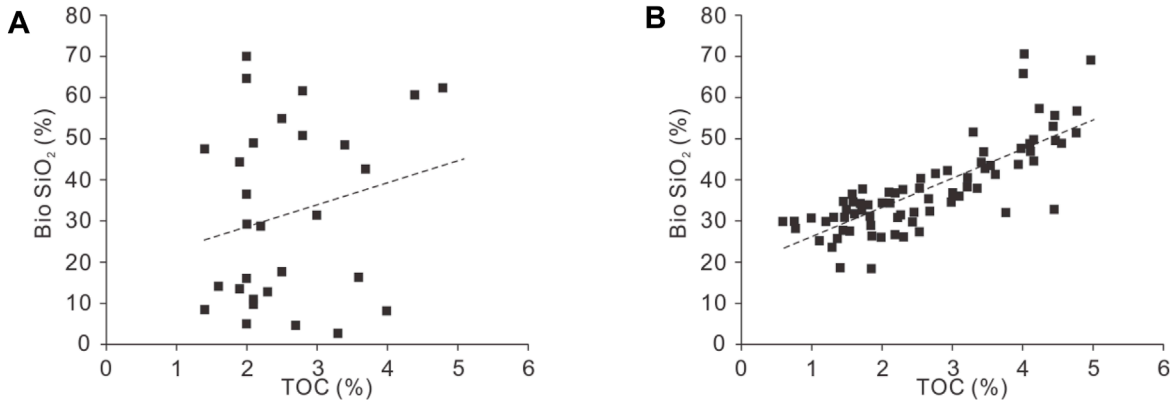

FIGURE 6
Cross-plot of TOC and Bio SiO_2 content in the Devonian-Mississippian black shale (Ross and Marc Bustin, 2009) **(A)** and Ordovician-Silurian black shale **(B)**.

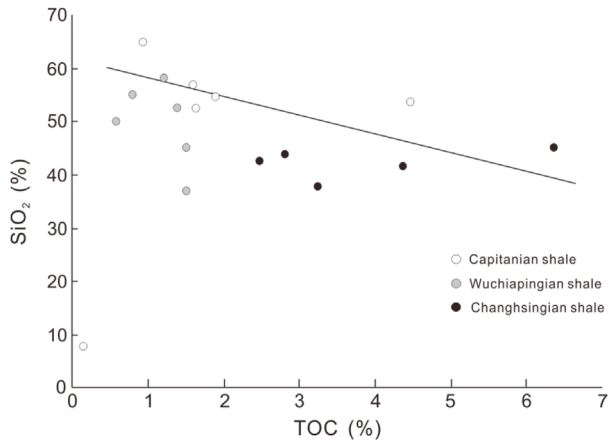

FIGURE 7
Correlation between TOC and SiO_2 content in black shale.

Paleo-ocean productivity

The productivity of marine surface organisms depends on the richness of nutrients in the surface water. The richer the nutrients, the more prosperous the organisms are, and the stronger the carbon production capacity of photosynthesis, resulting in greater productivity. The elements that can reflect the nutritional level of water include N, P, Fe, Cu, Ni, and Zn (Tribovillard et al., 2006). N and P are greatly affected by recycling and later diagenesis, while Fe are influenced by carbonate dissolution and recrystallization, etc., which make them unreal. Cu, Zn, and Ni as nutrient elements, combine with organic matter or form organic complexes for precipitation and burial, and high levels of Cu, Zn, and Ni reflected higher paleo-productivity (Tribovillard et al., 2006; Fathy et al., 2018). Therefore, Cu, Zn, and Ni can be used as indicators to reflect the level of ancient productivity. Another way to characterize the primary productivity of water surface is through the organic carbon flux of the water mass. High productivity enhances the organic carbon flux of the water mass. Organic carbon forms a local sulfate reduction microenvironment through complexation with trace metal elements or decomposition of organic matter, resulting in the precipitation of certain trace metal elements. The higher the organic carbon flux of the water mass, the greater the burial amount of certain trace metal elements.

In addition to hydrothermal activities, the main sources of these nutrients are biogenic and terrigenous, only biogenic elements can reflect the change of paleoproductivity. Before using these trace elements, the influence of terrestrial sources should be eliminated, and Ti or Al should be used to correct the above elements (Taylor and McLennan, 1985). The formula is:

$$X_{xs} = X_{total} - Ti_{total} \times (X/Ti)_{PAAS}$$

X_{xs} represents the excess value of X, which is obtained by Ti correction of the trace element content in the sample using the trace element content in PAAS. Xtotal is the total element content of the tested rock sample, and $(X/Ti)_{PAAS}$ represents the ratio of element content to Ti in PAAS. The (X/Ti) PAAS used is quoted from Taylor and McLennan (1985). If the calculation result is positive, it indicates that the element is relatively PAAS and exhibits marine autogenesis enrichment or volcanic hydrothermal enrichment. If the calculation result is negative, it indicates that the content of this element in the sample is mainly contributed by terrestrial materials.

The correlation between Ba and Mo and organic carbon flux in water mass is significant, which can reflect surface productivity. Dymond et al. (1992) established for the first time a calculation model for surface productivity using Ba as an indicator, using data obtained from sediment traps. The sources of Ba mainly include biogenic barium and terrestrial barium. Only the portion of Ba contributed by the source of students can reflect primary productivity. The calculation formula for biogenic Ba (Ba_{bio}) is consistent with the formula for excess trace elements. High marine productivity results in a large amount of organic carbon input, forming a large amount of hydrogen sulfide, which reacts with molybdate to form thiomolybdate, and is buried together with iron

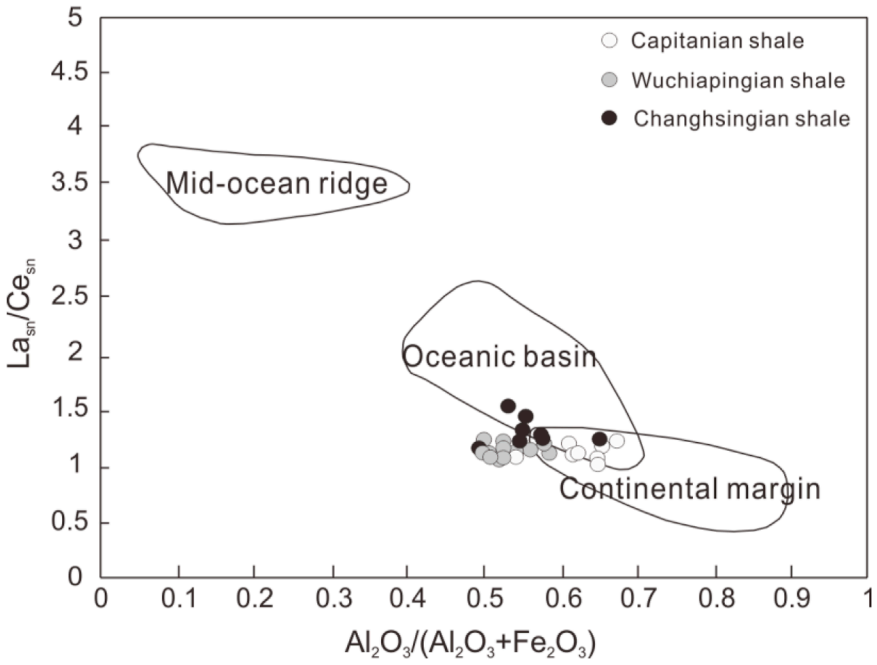

FIGURE 8
Correlation between $Al_2O_3/(Al_2O_3+Fe_2O_3)$ and La_{sn}/Ce_{sn} content in black shale (modiated from Wang et al., 2016).

sulfides and organic matter. The more organic carbon is input, the more Mo is deposited and buried. The advantage of Mo as an input parameter for organic carbon is that it is less affected by later changes, as the binding of iron sulfides to Mo is irreversible.

Cu_{bio}, Zn_{bio}, Ni_{bio}, and Ba_{bio} are used to reflect the paleo-productivity evolution of black shale (Shen et al., 2014). All elements are corrected by Ti, and negative excess element values are removed. The changes in paleo-marine productivity of the Capitanian-Changhsingian black shale obtained in the end are shown in Figure 9. The productivity of the ancient ocean corresponding to the Capitanian black shale is relatively high, while the productivity of the Wuchiapingian stage paleo ocean has decreased. In the early Changhsingian stage, the productivity of paleo-oceans significantly increased again. Overall, volcanic tuff has a significant promoting effect on the productivity of paleo-oceans. Further comparison between the evolution of paleo-productivity and the distribution characteristics of TOC reveals a consistent correspondence between high biological productivity and high organic matter accumulation. However, in the Wuchiapingian stage, the changes in productivity are not as significant as those in total organic carbon. The productivity has a controlling effect on organic carbon enrichment, but it is not the only controlling factor for organic carbon enrichment.

In recent years, many studies suggested that the efficient indicator for evaluating shale redox conditions is the U/Th ratio (Jones and Manning, 1994), and there is a significant correlation between TOC value and U/Th ratio. However, previous studies of the Permian Shanxi Formation transitional shale in North China suggested that the shale intervals heavily disturbed by terrestrial debris generally have lower U/Th ratios and poor correlation with TOC (Zhang et al., 2021). Taking this study as an example (Figure 10): The overall U/Th ratio is relatively low, and there is no trend of changes in redox conditions at different stages.

The results indicate that V/Cr is significantly better than U/Th and Ni/Co in reflecting the changes in redox conditions in the study area. Under the 3rd-order sequence framework, V/Cr well reflects the trend of change, with SQ2's V/Cr ranging from 1.40 to 3.77, with an average of 2.41 (n = 13), SQ3's V/Cr ranging from 1.09 to 2.89, with an average of 2.23 (n = 10), and SQ4's V/Cr ranging from 1.15 to 2.28, with an average of 1.64 (n = 12). Except for SQ2, the high value range of V/Cr is inconsistent with the development location of black shale, suggesting that the dysoxic and anoxic environment is not the only controlling factor for the development of black shale.

The Guadalupian-Lopingian boundary (G-LB) is a critical period in the development of Earth's history, during which the Earth's climate system experienced the disappearance of Late Paleozoic ice chambers and transitioned to Mesozoic greenhouses, accompanied by a series of major geological events such as the extinction of biological clusters (Stanley and Yang, 1994; Wignall and Bond, 2023), the eruption of Emeishan basalt (Sun et al., 2010), and a significant drop in sea-level to the lowest point of the Phanerozoic era (Haq and Schutter, 2008; Shen et al., 2019; Zhao et al., 2019). These events have more or less affected the global carbon cycle and are recorded in the inorganic carbon isotope changes of marine carbonate rocks (Wang et al., 2004; Shen et al., 2013). Therefore, carbon isotopes can also better reflect the global or regional changes in redox conditions of seawater during the Capitanian-Changhsingian stage. The results of intensive carbon isotope testing in the study area and other regions of South China (Figure 11) show that in the late Capitanian stage (SQ2), carbon isotopes showed a significant "negative shift". This phenomenon existed in multiple outcrops in the Upper Yangtze region, indicating

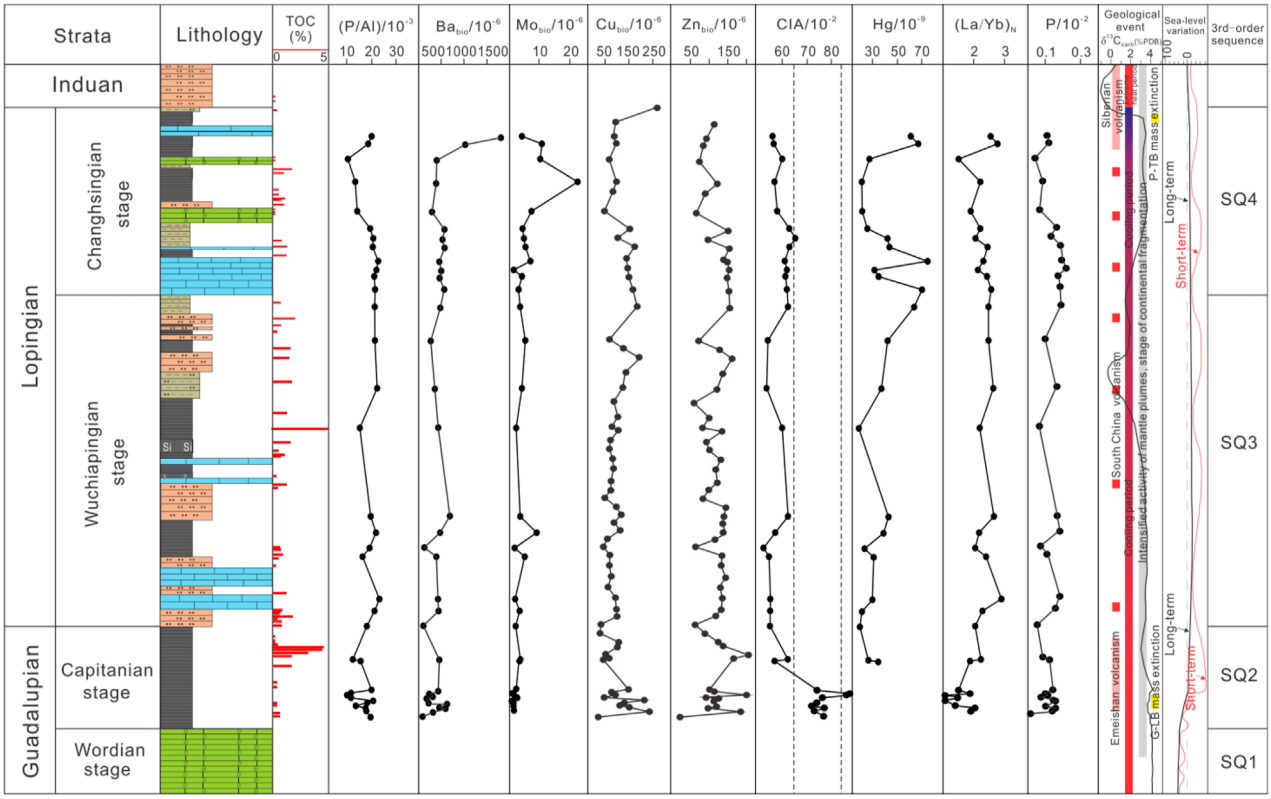

FIGURE 9
Comprehensive column for the paleo-productivity proxies during Guadalupian-Lower Triassic in the studied outcrop. Sea-level data are from Haq and Schutter (2008). Geological events are from Isozaki (2009), Wignall et al. (2009), Shen et al. (2013) and Chen et al. (2013). Paleo-redox condition under sequence framework.

the existence of regional anoxic events in seawater during this period, In the late SQ3-early SQ4 period, there was also a common phenomenon of negative carbon isotope shift in the Upper Yangtze region, indicating that seawater had regional anoxic characteristics during this period (Figure 12).

Organic matter accumulation is a complex physical-chemical process that involves many factors, such as redox condition of bottom seawater, sedimentation rate, productivity of surface water, and geological event. The main controlling factors for organic matter enrichment in modern and paleo marine sediments have been extensively discussed over the past 30 years (Pedersen et al., 1990; Arthur and Sageman, 1994; Wei et al., 2012; Ding et al., 2018). Three fundamental models have been identified for the accumulation of organic matter in organic-rich sediments: (1) enhanced organic productivity, (2) enhanced organic matter preservation, associated with reducing conditions and (3) low sedimentation rate (minimal detrital dilution). Sea-level fluctuations appear to exert a fundamental control on all three factors and therefore on organic matter accumulation. Currently, it is generally believed that organic matter enrichment is closely related to the preservation of large-scale biogenetic material, and the prerequisite for large-scale biogenetic material preservation is favorable sedimentary-burial conditions (such as anoxic and appropriate sedimentation rate). Consequently, the controlling factors for organic matter enrichment can be summarized as primary productivity and favorable preservation conditions in the marine surface. The productivity school, represented by Pedersen et al. (1990), Sageman et al. (2003), and Gallego-Torres et al. (2007), believes that organic matter accumulation is mainly controlled by the biological productivity of the ocean surface, and the impact of water redox properties is limited. The typical representative is the rising ocean currents on the continental margin. The oxidation-reduction school represented by Arthur and Sageman (1994) and Mort et al. (2007) believes that low marine surface productivity can also form organic rich sediments in hypoxic environments, especially in sulfide environments, with modern anoxic basins such as the Black Sea and Cretaceous marine anoxic events as typical representatives. Scholars such as Ibach (1982) and Morton et al. (2000) believe that an appropriate sedimentation rate is the key factor causing organic matter enrichment, and either too high or too low sedimentation rates are not conducive to organic matter enrichment.

From a global perspective, this area is located in the southwestern part of the South China during the Capitanian stage (Figure 13). Overall, SQ2-SQ4 has experienced one glacial event (Kamura glacial event), two biotic extinction events (G-LB and P-TB biotic extinction events), and two anoxic events (late Capitanian stage, late Wuchiapingian stage-early Changhsingian stage), Three major volcanic activities (Emeishan Igneous Province, South China Acidic Volcanic Activity, and Siberian Igneous

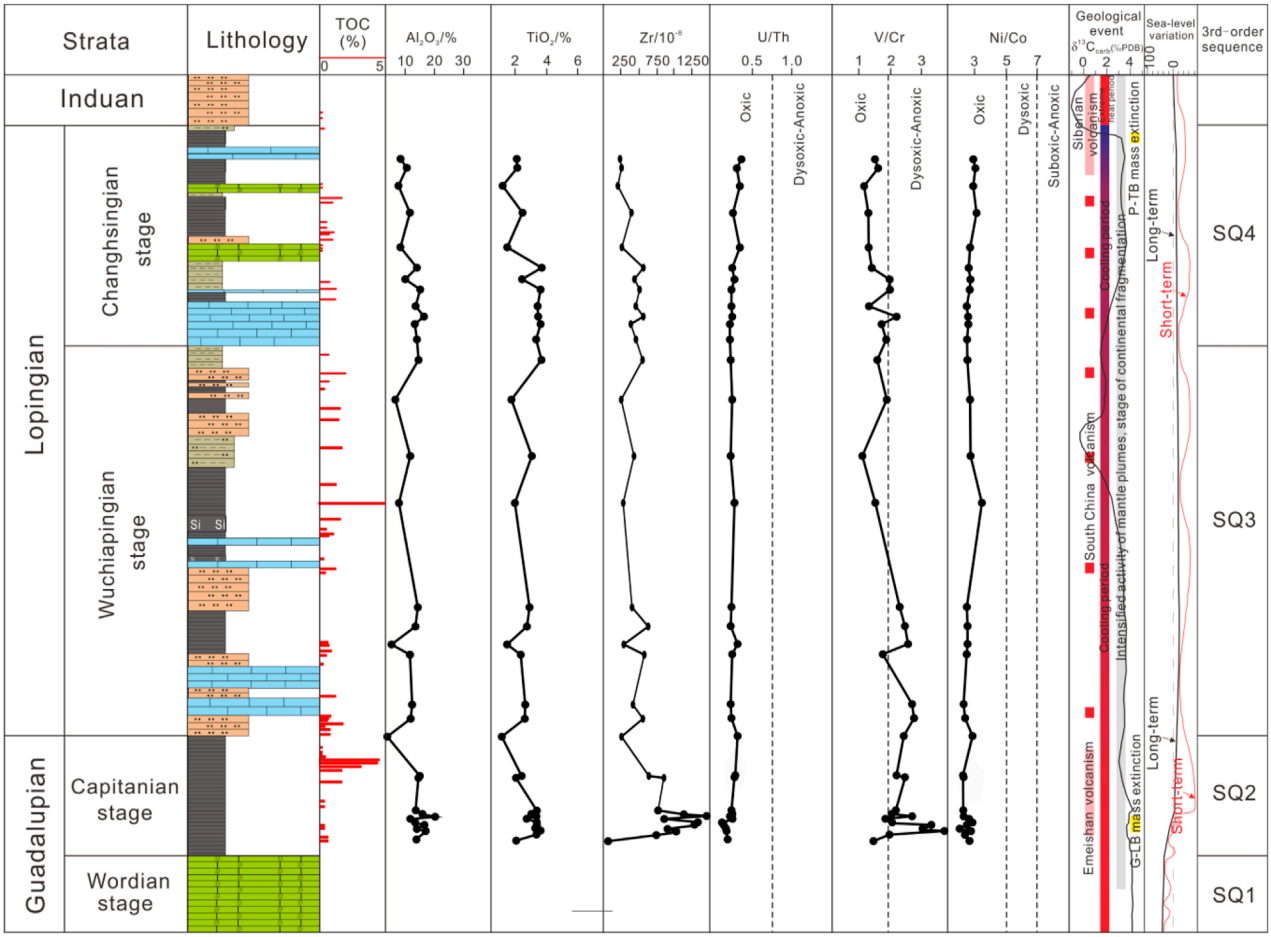

FIGURE 10
Comprehensive column for the terrestrial input and paleo-redox proxies during Guadalupian-Lower Triassic in the studied outcrop. Sea-level data are from Haq and Schutter (2008). Geological events are from Isozaki (2009), Wignall et al. (2009), Shen et al. (2013) and Chen et al. (2013).

Province). During this period, global sea levels experienced a period of "one regression and one transgression".

The Upper Yangtze region, where the study area is located, was dominated by shallow carbonate platform environment in the late Wordian stage before SQ2 sedimentation. The water in the entire area is in an oxic environment, characterized by moderate paleo-productivity and shallow water depth. Due to the seafloor expansion superimposed by the Kamura event (Figure 14), the global sea level of the Capitanian stage where SQ2 is located continuously decreased, reaching the lowest point in geological history by the end of the Capitanian stage (Haq and Schutter, 2008). Due to the volcanic ash formed by the eruption of the Emeishan Large Igneous Province, which is rich in nutrients such as Fe, P, N, Si, and Mn, it can promote the proliferation of algae and other organisms, and improve the primary productivity of surface seawater, During this period, due to the extensional rift activity induced by the Emeishan Large Igneous Province, the water in the rift area has rapidly deepened, resulting in a anoxic environment in intra-platform basin and shelf around extensional rift area. Meanwhile, the end of the glacial event is conducive to a significant rise in sea level, creating a hypoxic environment. The ocean is strongly retained, controlled by the upwelling of anoxic bottom seawater, and a large amount of organic carbon has been deposited and preserved due to the G-LB extinction event.

During SQ3, the extensional rift activity stagnated, and the differences in sedimentary landforms gradually disappeared due to the enhancement of terrestrial supply. The global sea-level further decreased, and the water conditions gradually changed from anoxic to dysoxic. In the later stage, they evolved into oxic conditions (Figure 14). Multiple periods of acidic volcanic activity in South China have maintained a high level of paleo-productivity in seawater. Under dysoxic conditions, organic matter can still be enriched in large quantities, forming the Wuchiapingian black shale. In the early stage of SQ4, the entire Changhsingian stage area was dominated by platform environment, with low sea-level and high paleo-productivity, all of which were in an oxic environment. However, at this time, it is a anoxic event of bottom water in deep sea, and the sedimentary paleo-geomorphology in the study area cannot cater to this period of anoxic event and does not have the conditions for organic matter enrichment. Accompanied by the Emeishan Rift Movement, the extensional subsidence activity resumed, and the water in the late SQ4 extensional subsidence area deepened sharply

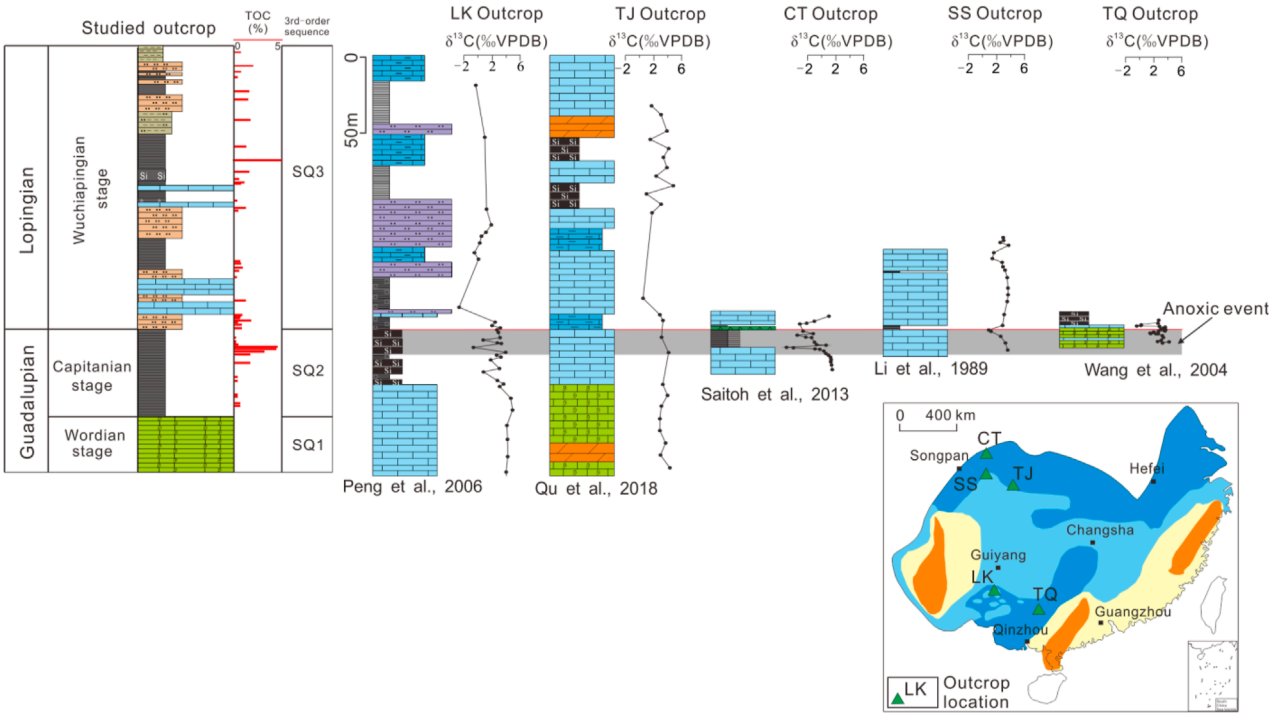

FIGURE 11
Comparison of carbon isotopes at the Guadalupian-Lopingian boundary (G-LB) between the studied outcrop and other typical outcrops in South China (Li et al., 1989; Wang et al., 2004; Peng et al., 2006; Saitoh et al., 2013; Qu et al., 2018).

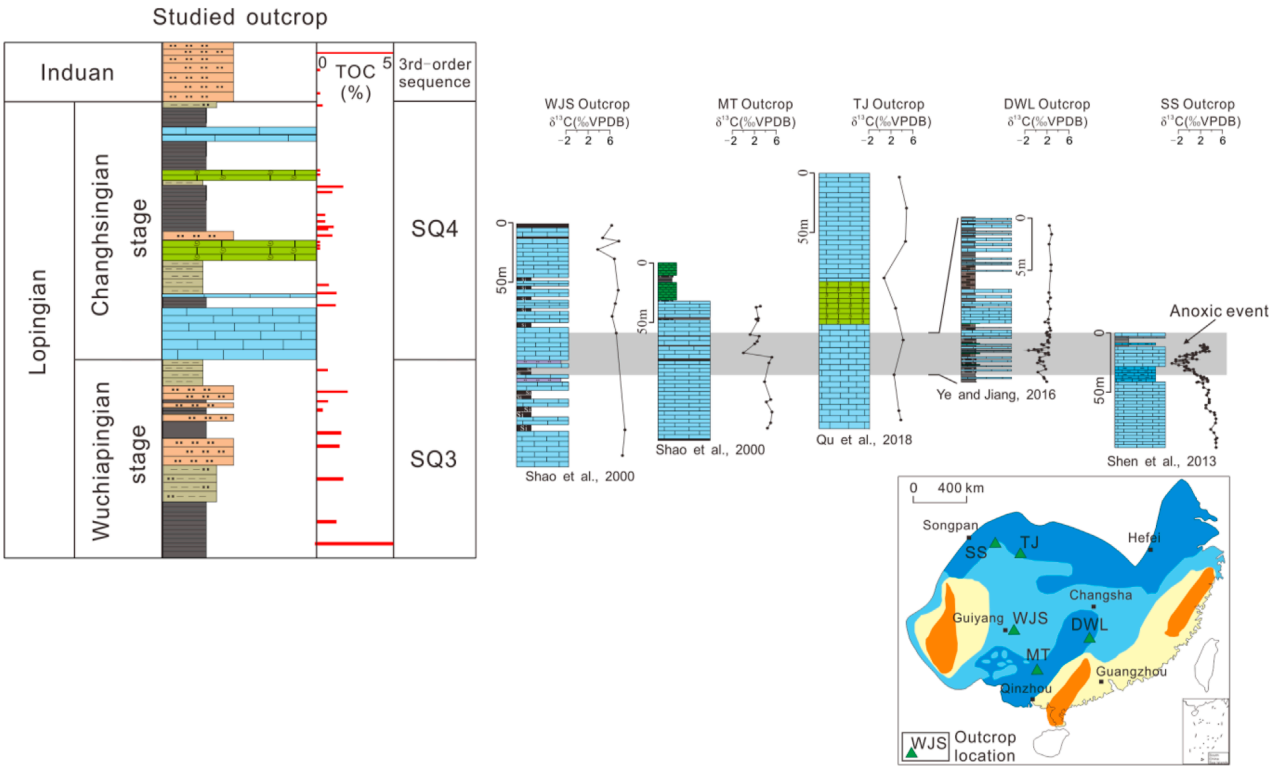

FIGURE 12
Comparison of carbon isotopes at the Wuchiapingian-Changhsingian boundary between the studied outcrop and other typical outcrops in South China. Organic matter enrichment and evolution model under sequence framework (Shao et al., 2000; Shen et al., 2013; Ye and Jiang, 2016; Qu et al., 2018).

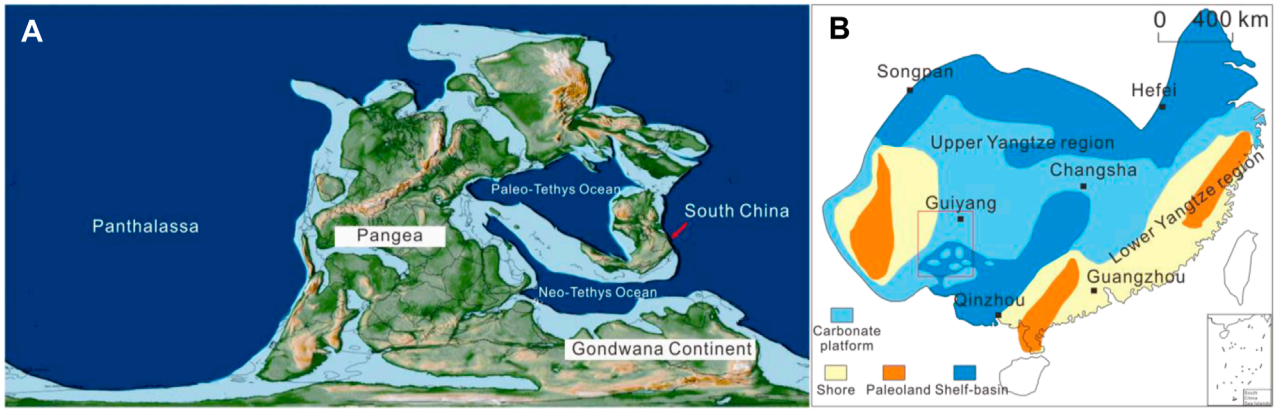

FIGURE 13
Paleogeographic characteristics during Guadalupian stage. **(A)** Global paleogeographic distribution (Scotese, 2016). **(B)** Paleogeographic characteristics of South China during Guadalupian stage (Qu et al., 2018).

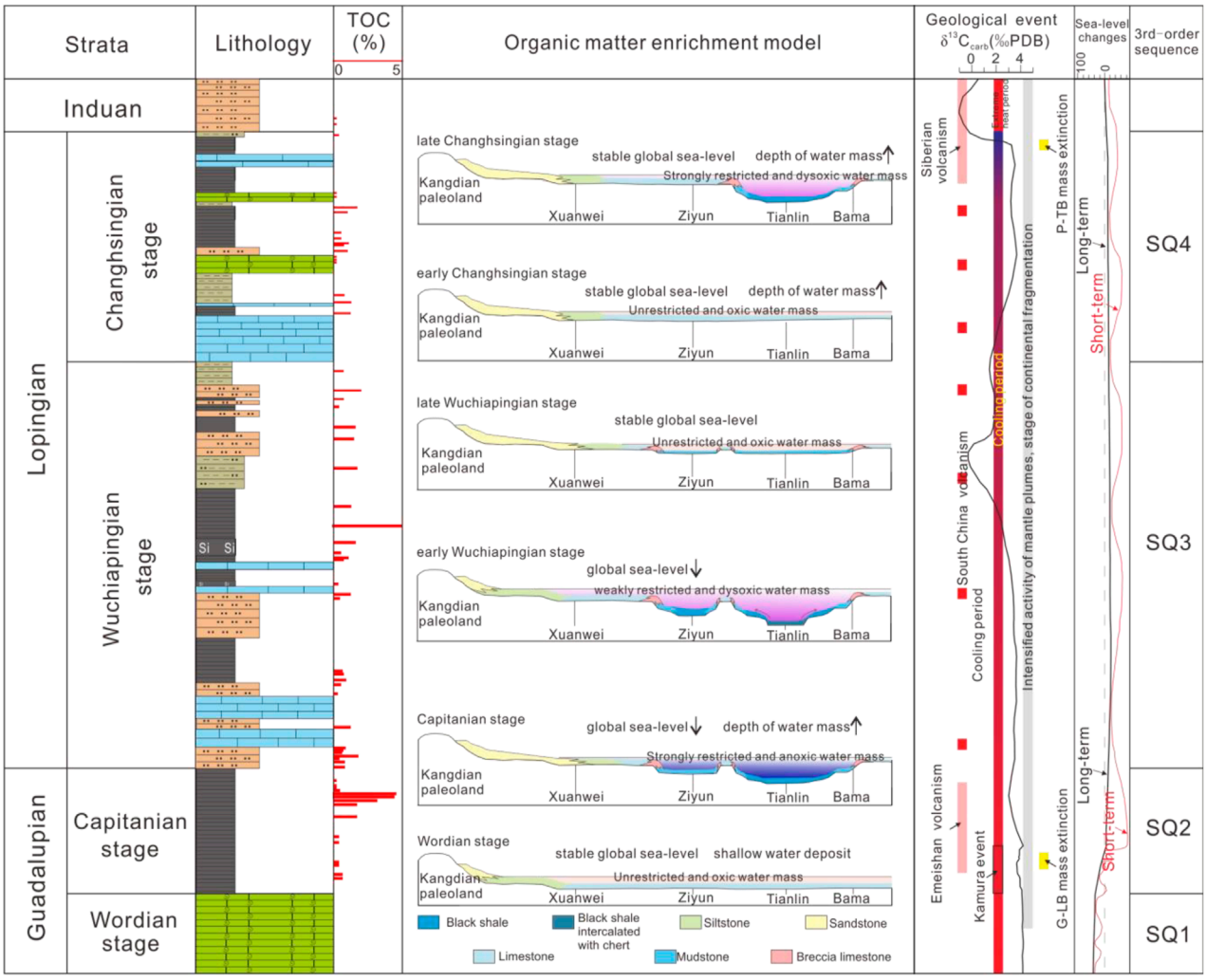

FIGURE 14
Organic matter enrichment models within the 3rd-order sequence framework during Guadalupian-Lower Triassic in the studied outcrop. Sea-level data are from Haq and Schutter (2008). Geological events are from Isozaki (2009), Wignall et al. (2009), Shen et al. (2013) and Chen et al. (2013).

again, with a sharp increase in ocean retention. The dysoxic water conditions resulted in the preservation of large-scale organic matter, forming the black shale during the Changhsingian stage (Figure 14).

Conclusion

1) The Permian Capitanian-Changhsingian black shale in the Northern Nanpanjiang Basin was formed in continental slope and marginal-sea sediments near the continent in the intra-platform basin. The SiO_2 content of the Capitanian-Changhsingian black shale is lower than that of the Ordovician-Silurian black marine shale and shows a gradually decreasing trend. The silicon in the black shale of the Capitanian stage, Wuchiapingian stage and Changhsingian stage in the study area is of non-hydrothermal origin, while the majority of the Capitanian stage is biogenic silicon. The TiO2 and MnO content of the Capitanian-Changhsingian black shale is significantly higher than that of the Ordovician-Silurian shale, and its major elemental composition is similar to that of siliceous rocks formed by volcanic biochemical processes.
2) The factors controlling the Capitanian black shale deposition are the rapidly deepening water mass of extensional rifts and the high productivity induced by volcanic ash in the major igneous provinces, as well as the global anoxic event represented by "negative carbon isotope shift". The factors controlling the Changhsingian black shale deposition are the deepening of water mass under the reactivation of extensional rifts, resulting in a dysoxic environment, and the high productivity maintained by volcanic activity in South China. The Wuchiapingian black shale was formed under dysoxic conditions under the stagnation of extensional activity, and intermittent volcanic activity in South China maintained the high paleo-productivity level of the Wuchiapingian stage.

Data availability statement

The original contributions presented in the study are included in the article/Supplementary Material, further inquiries can be directed to the corresponding author.

Author contributions

HZ: Conceptualization, Funding acquisition, Investigation, Visualization, Writing–original draft. JC: Investigation, Methodology, Project administration, Supervision, Writing–original draft. BL: Formal Analysis, Supervision, Validation, Writing–original draft. YC: Formal Analysis, Methodology, Writing–review and editing. QZ: Data curation, Resources, Software, Writing–review and editing. YM: Data curation, Investigation, Writing–review and editing. XF: Formal Analysis, Supervision, Writing–review and editing. QY: Supervision, Validation, Writing–review and editing.

Funding

The author(s) declare that financial support was received for the research, authorship, and/or publication of this article. The research was supported by the Guizhou Provincial Fund Project [Grant No. (2022)ZD005] and Guizhou Provincial Fund Project [Grant No. (2023)-344].

Conflict of interest

Author BL was employed by Ltd.

The remaining authors declare that the research was conducted in the absence of any commercial or financial relationships that could be construed as a potential conflict of interest.

Publisher's note

References

Algeo, T. J., and Maynard, J. B. (2004). Trace element behavior and redox facies in core shales of Upper Pennsylvanian Kansas-type cyclothems. *Chem. Geol.* 206, 289–318. doi:10.1016/j.chemgeo.2003.12.009

Arthur, M. A., and Sageman, B. B. (1994). Marine black shales: depositional mechanisms and environments of ancient deposits. *Annu. Rev. Earth Planet. Sci.* 22, 499–551. doi:10.1146/annurev.ea.22.050194.002435

Bai, L., Duan, L., Gao, Z., Ma, G., Yang, A., Liu, Z., et al. (2023). Controlling effect of shale pore connectivity on the adsorption state of shale gas: a case study of continental shale of Jurassic Ziliujing Formation, Sichuan Basin. *Energy fuels.* 37, 14891–14905. doi:10.1021/acs.energyfuels.3c02721

Bao, S. X., Zhou, H. Y., Peng, X. T., Ji, F. W., and Yao, H. Q. (2008). Geochemistry of REE and yttrium in hydrothermal fluids from the Endeavour segment, Juan de Fuca Ridge. *Geochem. Journey.* 42 (4), 359–370. doi:10.2343/geochemj.42.359

Cai, G., Gu, Y., Fu, Y., Jiang, Y., Wei, Z., Wang, Z., et al. (2023b). Pore system classification of Jurassic Da'anzhai Member lacustrine shale: insight from pore fluid distribution. *Energy Explor. Exploitation* 0 (0), 900–921. doi:10.1177/01445987231154613

Cai, G., Gu, Y., Jiang, Y., and Wang, Z. (2023a). Pore structure and fluid evaluation of deep organic-rich marine shale: a case study from Wufeng–Longmaxi Formation of Southern Sichuan Basin. *Appl. Sci.* 13, 7827. doi:10.3390/app13137827

Chen, B., Joachimski, M. M., Shen, S. Z., Lambert, L. L., Lai, X. L., Wang, X. D., et al. (2013). Permian ice volume and palaeoclimate history: oxygen isotope proxies revisited. *Gondwana Res.* 24 (2013), 77–89. doi:10.1016/j.gr.2012.07.007

Ding, J., Zhang, J., Tang, X., Huo, Z., Han, S., Lang, Y., et al. (2018). Elemental geochemical evidence for depositional conditions and organic matter enrichment of black rock series strata in an inter-platform basin: the lower carboniferous datang formation, Southern Guizhou, Southwest China. *Minerals* 8 (11), 480–509. doi:10.3390/MIN8110509

Dong, D., Qiu, Z., Zhang, L., Li, S., Zhang, Q., Li, X., et al. (2021). Progress on sedimentology of transitional facies shales and new discoveries of shale gas. *Acta Sedimentol. Sin.* 39 (1), 29–45. doi:10.14027/j.issn.1000-0550.2021.002

Dymond, J., Suess, E., and Lyle, M. (1992). Barium in deep-sea sediment: a geochemical proxy for paleoproductivity. *Paleoceanography* 7 (2), 163–181. doi:10.1029/92PA01080

Fan, C. H., Nie, S., Li, H., Radwan, A. E., Pan, Q. C., Shi, X. C., et al. (2024). Quantitative prediction and spatial analysis of structural fractures in deep shale gas reservoirs within complex structural zones: a case study of the Longmaxi Formation in the Luzhou area, southern Sichuan Basin, China. *J. Asian Earth Sci.* 263, 106025. doi:10.1016/j.jseaes.2024.106025

Fang, R., Jiang, Y., Sun, S., Luo, Y., Qi, L., Dong, D., et al. (2023). Controlling factors of organic matter accumulation and lacustrine shale distribution in Lianggaoshan Formation, Sichuan Basin, SW China. *Front. Earth Sci.* 11, 1218215. doi:10.3389/feart.2023.1218215

Fathy, D., Wagreich, M., Gier, S., Mohamed, R. S. A., Zaki, R., and El Nady, M. M. (2018). Maastrichtian oil shale deposition on the southern Tethys margin, Egypt: insights into greenhouse climate and paleoceanography. *Palaeogeogr. Palaeoclimatol. Palaeoecol.* 505, 18–32. doi:10.1016/j.palaeo.2018.05.017

Gallego-Torres, D., Martínez-Ruiz, F., Paytan, A., Jiménez-Espejo, F. J., and Ortega-Huertas, M. (2007). Pliocene-holocene evolution of depositional conditions in the eastern mediterranean: role of anoxia vs. productivity at time of sapropel deposition. *Palaeogeogr. Palaeoclimatol. Palaeoecol.* 246 (2–4), 424–439. doi:10.1016/j.palaeo.2006.10.008

Ge, X. Y., Mou, C. L., Yu, Q., Liu, W., Meng, X., He, J. L., et al. (2021). A study on the enrichment of organic materials in black shales of the wufeng to longmaxi formations in eastern Sichuan Basin. *Sediment. Geol. Tethyan Geol.* 41 (3), 418–435. doi:10.19826/j.cnki.1009-3850.2020.12001

Gu, Y., Hu, D., Wei, Z., Liu, R., Hao, J., Han, J., et al. (2022). Sedimentology and geochemistry of the upper permian linghao formation marine shale, central Nanpanjiang Basin, SW China. *Front. Earth Sci.* 10, 914426. doi:10.3389/feart.2022.914426

Halamić, J., Marching, V., and Goričan, Š. (2005). Jurassic radiolarian cherts in north-western Croatia: geochemistry, material provenance and depositional environment. *Geol. Carpathica* 56 (2), 123–136. doi:10.1111/j.1472-4669.2005.00045.x

Han, H., Dai, J., Guo, C., Zhong, N., Pang, P., Ding, Z., et al. (2021). Pore characteristics and factors controlling lacustrine shales from the Upper Cretaceous Qingshankou Formation of the Songliao Basin, Northeast China: a study combining SEM, low-temperature gas adsorption and MICP experiments. *Acta Geol. Sin. Engl. Ed.* 95 (2), 585–601. doi:10.1111/1755-6724.14419

Haq, B. U., and Schutter, S. R. (2008). A chronology of Paleozoic sea-level changes. *Science* 322, 64–68. doi:10.1126/science.1161648

Hu, T., Pang, X., Wang, Q., Jiang, S., Wang, X., Huang, C., et al. (2018). Geochemical and geological characteristics of permian lucaogou formation shale of the well ji174, jimusar sag, junggar basin, China: implications for shale oil exploration. *Geol. J.* 2017, 2371–2385. doi:10.1002/gj.3073

Ibach, L. E. J. (1982). Relationship between sedimentation rate and total organic carbon content in ancient marine sediments. *AAPG Bulletin.* 66 (2), 170–188. doi:10.1306/03B59A5D-16D1-11D7-8645000102C1865D

Isozaki, Y. (2009). Integrated "plume winter" scenario for the double-phased extinction during the Paleozoic–Mesozoic transition: the G-LB and P-TB events from a Panthalassan perspective. *J. Asian Earth Sci.* 36 (2009), 459–480. doi:10.1016/j.jseaes.2009.05.006

Jiang, Y., Chen, L., Qi, L., Luo, M., Chen, X., Tao, Y., et al. (2018). Characterization of the lower silurian longmaxi marine shale in changning area in the South sichuan basin, China. *Geol. J.* 53, 1656–1664. doi:10.1002/gj.2983

Jiang, Y., Song, Y., Qi, L., Chen, L., Tao, Y., Gan, H., et al. (2016). Fine lithofacies of China's marine shale and its logging prediction: a case study of the Lower Silurian Longmaxi marine shale in Weiyuan area, southern Sichuan Basin,China. *Earth Sci. Front.* 23 (1), 107–118. doi:10.13745/j.esf.2016.01.010

Jiao, F., Wen, S., Liu, X., Xiong, X., Li, S., Gu, Y., et al. (2023). Research progress in exploration theory and technology of transitional shale gas in the Ordos Basin. *Nat. Gas. Ind.* 43 (4), 11–23. doi:10.3787/j.issn.1000-0976.2023.04.002

Jones, B., and Manning, D. A. C. (1994). Comparison of geochemical indices used for the interpretation of palaeoredox conditions in ancient mudstones. *Chem. Geol.* 111 (1–4), 111–129. doi:10.1016/0009-2541(94)90085-X

Labani, M. M., Rezaee, R., Saeedi, A., and Al Hinai, A. (2013). Evaluation of pore size spectrum of gas shale reservoirs using low pressure nitrogen adsorption, gas expansion and mercury porosimetry: a case study from the Perth and Canning Basins, Western Australia. *J. Petroleum Sci. Eng.* 112, 7–16. doi:10.1016/j.petrol.2013.11.022

Lai, X., Wang, W., Wignall, P. B., Bond, D. P. G., Jiang, H., Ali, J. R., et al. (2008). Palaeoenvironmental change during the end-Guadalupian (Permian) mass extinction in sichuan, China. *Palaeogeogr. Palaeoclimatol. Palaeoecol.* 269 (1-2), 78–93. doi:10.1016/j.palaeo.2008.08.005

Li, H. (2023). Coordinated development of shale gas benefit exploitation and ecological environmental conservation in China: a mini review. *Front. Ecol. Evol.* 11, 1232395. doi:10.3389/fevo.2023.1232395

Li, H. Z., Zhai, M. G., Zhang, L. C., Gao, L., Yang, Z. J., Zhou, Y. Z., et al. (2014). Distribution, microfabric, and geochemical characteristics of siliceous rocks in central orogenic belt, China: implications for a hydrothermal sedimentation model. *Sci. World J.* 780910 (4), 1–25. doi:10.1155/2014/780910

Li, Z., Zhan, L., Dai, J., Jin, R., Zhu, X., Zhang, J., et al. (1989). *Research on the Permian Triassic biostratigraphy and event stratigraphy in northern Sichuan and southern Shaanxi*. Beijing: Beijing Geological Publishing House, 435.

Lin, M., Xi, K., Cao, Y., Liu, Q., Zhang, Z., and Li, K. (2021). Petrographic features and diagenetic alteration in the shale strata of the permian lucaogou formation, jimusar sag, junggar basin. *J. Petroleum Sci. Eng.* 203, 108684. doi:10.1016/j.petrol.2021.108684

Liu, W., Gao, P., Xiao, X., Zhao, Y., Xing, Y., and Li, J. (2024). Variable depositional environments and organic matter enrichment of Early Cambrian shales in the Middle Yangtze region, South China. *J. Asian Earth Sci.* 259 (2024), 105874. doi:10.1016/j.jseaes.2023.105874

Liu, Z., Yan, D., Yuan, D., Niu, X., and Fu, H. (2022). Multiple controls on the organic matter accumulation in early Cambrian marine black shales, middle Yangtze Block, South China. *J. Nat. Gas Sci. Eng.* 100 (2022), 104454. doi:10.1016/j.jngse.2022.104454

Loucks, R. G., Reed, R. M., Ruppel, S. C., and Jarvie, D. M. (2009). Morphology, genesis, and distribution of nanometer-scale pores in siliceous mudstones of the Mississippian Barnett Shale. *J. Sediment. Res.* 79 (12), 848–861. doi:10.2110/jsr.2009.092

Ma, K., Hu, S. Y., Wang, T. S., Zhang, B. M., Qin, S. F., Shi, S. Y., et al. (2017). Sedimentary environments and mechanisms of organic matter enrichment in the Mesoproterozoic Hongshuizhuang Formation of northern China. *Palaeogeogr. Palaeoclimatol. Palaeoecol.* 75, 176–187. doi:10.1016/j.palaeo.2017.02.038

Mei, M., Ma, Y., Deng, J., Chu, H., and Zheng, K. (2007). Sequence stratigraphy framework and paleogeographical setting of the Lo-ping of the Pemian of Dian-Qian-Gui Basin and its adjacent areas. *Sci. China Ser. D* 37 (5), 605–617. doi:10.3969/j.issn.1674-7240.2007.05.004

Milliken, K. L., Ergene, S. M., and Ozkan, A. (2016). Quartz types, authigenic and detrital, in the upper cretaceous eagle ford formation, South Texas, USA. *Sediment. Geol.* 339 (2016), 273–288. doi:10.1016/j.sedgeo.2016.03.012

Milliken, K. L., and Olson, T. (2017). Silica diagenesis, porosity evolution, and mechanical behavior in siliceous mudstones, Mowry Shale (Cretaceous), Rocky Mountains, U.S.A. *J. Sediment. Res.* 88, 366–387. doi:10.2110/jsr.2017.24

Mort, H. P., Adatte, T., Föllmi, K. B., Keller, G., Steinmann, P., Matera, V., et al. (2007). Phosphorus and the roles of productivity and nutrient recycling during oceanic anoxic event 2. *Geology.* 35 (6), 483–486. doi:10.1130/G23475A.1

Morton, R. A., Ward, G. H., and White, W. A. (2000). Rates of sediment supply and sea-level rise in a large coastal lagoon. *Marine Geology.* 167 (3–4), 261–284. doi:10.1016/S0025-3227(00)00030-X

Pedersen, T. F., and Calvert, S. E. (1990). Anoxia vs. Productivity: What Controls the Formation of Organic-Carbon-Rich Sediments and Sedimentary Rocks? *AAPG Bulletin.* 74 (1), 454–466. doi:10.1306/0C9B232B-1710-11D7-8645000102C1865D

Peng, B., Wang, Y., Fan, W., and Peng, T. (2006). Carbon isotope composition changes of Maokouian-Wuchiapingian and the environmental effect of Emeishan large igneous province at Lekang section, Guizhou Province. *Geochimica* 35 (2), 126–132. doi:10.19700/j.0379-1726.2006.02.002

Qiu, Z., and Zou, C. (2020). Unconventional Petroleum Sedimentology: Connotation and prospect. *Acta Sedimentol. Sin.* 38 (1), 1–29. doi:10.14027/j.issn.1000-0550.2019.116

Qu, H., Li, P., Luo, T., Guan, L., Fan, Y., and Wang, L. (2018). Carbon isotopic evolution characteristics and the geological significance of the Permian carbonate stratotype section in the Northern Upper-Yangtze Region, Southern China. *Acta Geol. Sin. Engl. Ed.* 92 (6), 2367–2381. doi:10.1111/1755-6724.13733

Ross, D. J. K., and Marc Bustin, R. (2009). The importance of shale composition and pore structure upon gas storage potential of shale gas reservoirs. *Mar. Petroleum Geol.* 26, 916–927. doi:10.1016/j.marpetgeo.2008.06.004

Sageman, B. B., Murphy, A. E., Werne, J. P., Straeten, C. A. V., and Lyons, T. W. (2003). A tale of shales: the relative roles of production, decomposition, and dilution in the accumulation of organic-rich strata, middle-upper devonian, Appalachian basin. *Chemical Geology.* 195 (1), 229–273. doi:10.1016/S0009-2541(02)00397-2

Saitoh, M., Isozaki, Y., Ueno, Y., Yoshida, N., Yao, J., and Ji, Z. (2013). Middle-Upper Permian carbon isotope stratigraphy at Chaotian, South China: Pre-extinction multiple upwelling of oxygen-depleted water onto continental shelf. *J. Asian Earth Sci.* 67–68, 51–62. doi:10.1016/j.jseaes.2013.02.009

Scotese, C. (2016). PALEOMAP PALEOATLAS FOR GPLATES AND THE PALEODATAPLOTTER PROGRAM. *50th Annu. GSA North-Central Sect. Meet.*, 275387. doi:10.1130/abs/2016NC-275387

Shao, L., Zhang, P., Dou, J., and Shen, S. (2000). Carbon isotope compositions of the Late Permian carbonate rocks in southern China: their variations between the Wujiaping and Changxing formations. *Palaeogeogr. Palaeoclimatol. Palaeoecol.* 161 (2000), 179–192. doi:10.1016/S0031-0182(00)00122-X

Shen, J., Zhou, L., Feng, Q., Zhang, M., Lei, Y., Zhang, N., et al. (2014). Paleo-productivity evolution across the Permian-Triassic boundary and quantitative calculation of primary productivity of black rock series from the Dalong Formation, South China. *Sci. China Earth Sci.* 57 (7), 1583–1594. doi:10.1007/s11430-013-4780-5

Shen, S., Cao, C., Zhang, H., Bowring, S. A., Henderson, C. M., Payne, J. L., et al. (2013). High-resolution $\delta^{13}C_{carb}$ chemostratigraphy from latest Guadalupian through earliest Triassic in South China and Iran. *Earth Planet. Sci. Lett.* 375 (2013), 156–165. doi:10.1016/j.epsl.2013.05.020

Shen, S., Zhang, H., Zhang, Y., Yuan, D., Chen, B., He, W., et al. (2019). Permian integrative stratigraphy and timescale of China. *Sci. China Earth Sci.* 62, 154–188. doi:10.1007/s11430-017-9228-4

Stanley, S. M., and Yang, X. (1994). A double mass extinction at the end of the Paleozoic Era. *Science* 266 (5189), 1340–1344. doi:10.1126/science.266.5189.1340

Sun, Y., Lai, X., Wignall, P. B., Widdowson, M., Ali, J. R., Jiang, H. S., et al. (2010). Dating the onset and nature of the Middle Permian Emeishan Large Igneous Province eruptions in SW China using conodont biostratigraphy and its bearing on mantle plume uplift models. *Lithos* 119 (1/2), 20–33. doi:10.1016/j.lithos.2010.05.012

Tan, J., Jiang, Y., Li, X., Ji, C., Gu, Y., and Wang, Z. (2024). Paleoenvironment of marine-continental transitional shales in the lower Permian Shanxi formation, southeastern Ordos Basin, China. *Energy Geosci.* 5 (2024), 100261. doi:10.1016/j.engeos.2023.100261

Taylor, S. R., and McLennan, S. M. (1985). *The continental crust: its composition and evolution*. Oxford: Blackwell Scientific Publications.

Tribovillard, N., Algeo, T. J., Baudin, F., and Riboulleau, A. (2012). Analysis of marine environmental conditions based on molybdenum-uranium covariation-Applications to Mesozoic paleoceanography. *Chem. Geol.* 324-325, 46–58. doi:10.1016/j.chemgeo.2011.09.009

Tribovillard, N., Algeo, T. J., Lyons, T., and Riboulleau, A. (2006). Trace metals as paleoredox and paleoproductivity proxies: An update. *Chem. Geol.* 232, 12–32. doi:10.1016/j.chemgeo.2006.02.012

Wang, E., Guo, T., Li, M., Xiong, L., Dong, X., Wang, T., et al. (2023). Reservoir characteristics and oil properties of a lacustrine shale system: Early Jurassic black shale from the Sichuan Basin, SW China. *J. Asian Earth Sci.* 242 (2023), 105491. doi:10.1016/j.jseaes.2022.105491

Wang, W., Cao, C., and Wang, Y. (2004). The carbon isotope excursion on GSSP candidate section of Lopingian-Guadalupian boundary. *Earth Planet. Sci. Lett.* 220 (2004), 57–67. doi:10.1016/S0012-821X(04)00033-0

Wang, X. D., Lv, X. B., Cao, X. F., Yuan, Q., Wang, Y. F., Liu, W., et al. (2016). Petrology and geochemistry of the banded iron formation of the Kuluketage Block, Xinjiang, NW China: Implication for BIF depositional setting. *Resour. Geol.* 66 (4), 313–334. CNKI:SUN:KCDZ.0.2014-S1-231. doi:10.1111/rge.12107

Wang, X. P., Wang, Q. Y., and An, X. Y. (2022). Characteristics of sedimentary environment and evolution of Permian in southern Sichuan Basin: An example from the profile of Gulin Bajiaocun in Sichuan Province. *Sediment. Geol. Tethyan Geol.* 42 (3), 398–412. doi:10.19826/j.cnki.1009-3850.2022.05009

Wang, Z., Huang, Z., Yao, J., and Ma, X. (2014). Characteristics and main progress of the stratigraphic chart of China and directions. *Acta Geosci. Sin.* 35 (3), 271–276. doi:10.3975/cagsb.2014.03.01

Wei, H., Chen, D., Wang, J., Yu, H., and Tucker, M. E. (2012). Organic accumulation in the lower Chihsia formation (Middle Permian) of South China: constraints from pyrite morphology and multiple geochemical proxies. *Palaeogeogr. Palaeoclimatol. Palaeoecol* 353–355 (2012), 73–86. doi:10.1016/j.palaeo.2012.07.005

Wei, W., Yu, W., Algeo, T. J., Herrmann, A. D., Zhou, L., Liu, J., et al. (2022). Boron proxies record paleosalinity variation in the North American Midcontinent Sea in response to Carboniferous glacio-eustasy. *Geology* 5, 537–541. doi:10.1130/G49521.1

Wignall, P. B., and Bond, D. P. G. (2023). The great catastrophe: causes of the Permo-Triassic marine mass extinction. *Natl. Sci. Rev.* 11 (1), nwad273. doi:10.1093/nsr/nwad273

Wignall, P. B., Sun, Y., Bond, D. P. G., Izon, G., Newton, R. J., Védrine, S., et al. (2009). Volcanism, mass extinction, and carbon isotope fluctuations in the Middle Permian of China. *Science* 324, 1179–1182. doi:10.1126/science.1171956

Xiong, G. Q., Liu, C. L., Dong, G. M., and Cui, W. (2021). A study of element geochemistry of mudstones of upper Ordovician Wufeng formation and lower Silurian Longmaxi formation in southern Daba Mountain. *Sediment. Geol. Tethyan Geol.* 41 (3), 399–417. doi:10.19826/j.cnki.1009-3850.2020.07001

Yamamoto, K. (1987). Geochemical characteristics and depositional environments of cherts and associated rocks in the Franciscan and Shimanto Terranes. *Sediment. Geol.* 52, 65–108. doi:10.1016/0037-0738(87)90017-0

Ye, Q., and Jiang, H. (2016). Conodont biostratigraphy and a negative excursion in carbonate carbon isotopes across the Wuchiapingian-Changhsingian boundary at the Dawoling Section, Hunan Province. *Earth Sci.* 41 (11), 1883–1892. doi:10.3799/dqkx.2016.130

Yin, H., Jiang, H., Xia, W., Feng, Q., Zhang, N., and Shen, J. (2014). The end-Permian regression in South China and its implication on mass extinction. *Earth-Science Rev.* 137 (2014), 19–33. doi:10.1016/j.earscirev.2013.06.003

Zhai, G., Wang, Y., Liu, G., Zhou, Z., Zhang, C., and Liu, X. (2020). Enrichment and accumulation characteristics and prospect analysis of the Permian marine continental multiphase shale gas in China. *Sediment. Geol. Tethyan Geol.* 40 (3), 102–117. doi:10.19826/j.cnki.1009-3850.2020.07003

Zhang, J., Li, X., Zhang, X., Zhang, M., Cong, G., Zhang, G., et al. (2018). Geochemical and geological characterization of marine-continental transitional shales from Longtan Formation in Yangtze area, South China. *Mar. Petroleum Geol.* 96, 1–15. doi:10.1016/j.marpetgeo.2018.05.020

Zhang, L. F., Dong, D. Z., Qiu, Z., Wu, C. J., Zhang, Q., Wang, Y. M., et al. (2021). Sedimentology and geochemistry of Carboniferous-Permian marine-continental transitional shales in the eastern Ordos Basin, North China. *Palaeogeogr. Palaeoclimatol. Palaeoecol.* 571, 110389. doi:10.1016/j.palaeo.2021.110389

Zhang, K., Song, Y., Jia, C., Jiang, Z., Han, F., Wang, P., et al. (2022). Formation mechanism of the sealing capacity of the roof and floor strata of marine organic-rich shale and shale itself, and its influence on the characteristics of shale gas and organic matter pore development. *Mar. Petroleum Geol.* 140, 105647. doi:10.1016/j.marpetgeo.2022.105647

Zhao, J., Jin, Z., Jin, Z., Geng, Y., Wen, X., and Yan, C. (2016). Applying sedimentary geochemical proxies for paleoenvironment interpretation of organic-rich shale deposition in the Sichuan Basin, China. *Int. J. Coal Geol.* 163, 52–71. doi:10.1016/j.coal.2016.06.015

Zhao, T. Y., Algeo, T. J., Feng, Q. L., Zi, J. W., and Xu, G. (2019). Tracing the provenanceof volcanic ash in Permian-Triassic boundary strata, South China: Constraints from inherited and syn-depositional magmatic zircons. *Palaeogeogr. Palaeoclimatol. Palaeoecol.* 516, 190–202. doi:10.1016/j.palaeo.2018.12.002

Zou, C., Zhu, R., Chen, Z., Ogg, J. G., Wu, S., Dong, D., et al. (2019). Organic-matter-rich shales of China. *Earth Sci. Rev.* 189, 51–78. doi:10.1016/j.earscirev.2018.12.002